

Article

# Correlation between Dielectric Loss and Partial Discharge of Oil-Pressboard Insulation

Yan Li <sup>1</sup> , Min Li <sup>2</sup> and Jun Xie <sup>1,\*</sup> 

<sup>1</sup> School of Electrical and Electronic Engineering, North China Electric Power University, Baoding 071003, China; yan.li@ncepu.edu.cn

<sup>2</sup> State Grid Baoding Electric Power Company Limited, Baoding 071000, China; limin\_sgcc@126.com

\* Correspondence: junxie@ncepu.edu.cn

**Abstract:** Dielectric loss  $\tan\delta$  and partial discharge (PD) are important indicators for status assessment of oil-pressboard insulation. The correlation characteristics between these two parameters has significance for understanding the material's degradation and helps to eliminate the information asymmetry for diagnostics. In this paper, the symmetric experimental platform is set up to measure the dielectric loss  $\tan\delta$  and PD for oil-pressboard insulation following the designed testing procedure consisted of raised and rested voltages. Three sets of samples with different water content were tested. The variation mechanism of  $\tan\delta$  with voltage is explained by proposed equivalent circuit, which introduced an asymmetric component representing defect part. PDs are found to be symmetric in the sinusoidal voltage cycles and their statistical parameters are calculated. Besides, the correlation between dielectric loss difference from raised voltage to rested voltage and PD is researched. Strong correlation is observed between dielectric loss and PD, which offers degradation insight for oil-pressboard insulation and helps to eliminate information asymmetry for material status diagnostics.

**Keywords:** correlation; dielectric loss; oil-pressboard insulation; partial discharge



**Citation:** Li, Y.; Li, M.; Xie, J.

Correlation between Dielectric Loss and Partial Discharge of Oil-Pressboard Insulation. *Symmetry* **2021**, *13*, 864. <https://doi.org/10.3390/sym13050864>

Academic Editor: Alexey Lukoyanov

Received: 22 April 2021

Accepted: 9 May 2021

Published: 12 May 2021

**Publisher's Note:** MDPI stays neutral with regard to jurisdictional claims in published maps and institutional affiliations.



**Copyright:** © 2021 by the authors. Licensee MDPI, Basel, Switzerland. This article is an open access article distributed under the terms and conditions of the Creative Commons Attribution (CC BY) license (<https://creativecommons.org/licenses/by/4.0/>).

## 1. Introduction

Oil-pressboard insulation material is widely used in transformers, bushings, capacitors, etc. [1–3]. Dielectric loss  $\tan\delta$  and partial discharge (PD) are the two parameters that are used to assess the insulation status [4–6]. As early as 1976, Takahashi E. et al. analyzed the PD characteristics for oil-paper under DC and AC voltages [7]. Later on, researchers studied the PD features under surge voltage [8,9]. Besides the recorded time-resolved data, statistical parameters are used for PD analysis [10,11]. Regarding dielectric loss, besides its own diagnostic function for insulation materials, Ruan J. et al. developed the inversion algorithm to obtain the oil-immersed paper resistivity from dielectric loss for insulation status assessment [12]. Frequency domain spectroscopy measurement is further developed based on dielectric loss to diagnose oil-pressboard [13].

The water content in the oil-pressboard may influence its insulation status, leading to different dielectric loss and/or PD behavior [14–16]. Przybylek P. et al. investigated the influence of cellulose insulation ageing and moistening on dielectric losses [17]. Cui Y. et al. proposed a distributed parameter model to reveal the correlation between moisture distribution and the dielectric response parameters of cellulose insulation [18]. Liao R. et al. performed quantitative diagnosis of moisture content in oil-paper insulation based on frequency domain spectroscopy [19].

The relation between PD and water ingress is also researched. Rowland S.M. et al. measured the PD development for wet oil-paper [20]. Ramya M. et al. found that water in pressboard papers makes the partial discharge inception voltage (PDIV) low and the PD occurred frequently, quickly leading to breakdown [21]. Župan T. et al. designed a capsule that can be used in the assessment of water content influence on the condition of

the oil-paper insulation [22]. Jiang J. et al. reported that there is a sharp reduction of PDIV or a sudden increase of PD intensity due to moisture in oil-paper insulation [23].

Although great effort has been devoted into oil-pressboard characteristics, to characterize its degradation based on single parameter, e.g., dielectric loss or PD, may create information asymmetry and lead to an incorrect result. Understanding their correlation offers insight into material's degradation mechanism and new tools for diagnostics, which helps to eliminate the information asymmetry in material assessment. This paper focuses on the correlation between dielectric loss  $\tan\delta$  and PD for oil-pressboard material, which was seldom researched by previous scholars. Parameters with strong correlation are identified in this paper, and the dielectric loss dependency upon PD is explained. The scientific goal is to explore the comprehensive degradation characteristics of oil-paper insulation and understand its mechanism, which is helpful for insulation/equipment condition diagnostics. In this paper, the oil-pressboard samples with different water content were prepared in this paper. The dielectric loss and PD for oil-pressboard insulation are measured simultaneously and their correlation is discussed.

This paper is organized, as follows. Section 2 describes the test setup. Section 3 gives the result of dielectric loss  $\tan\delta$  and PD separately for three samples with different water content. Section 4 discussed the correlation between these two parameters. Section 5 provides conclusions.

## 2. Test Setup and Measurement Procedure

### 2.1. Test Setup

The test model of oil-pressboard insulation was constructed, as in Figure 1, based on symmetry principle. The voltage electrodes are round plates with 400 mm diameter for high voltage and 500 mm diameter for grounding electrode, as in Figure 1a. The tested square oil-pressboard is from Weidmann and it has side length of 480 mm and 2 mm thickness, as in Figure 1b.

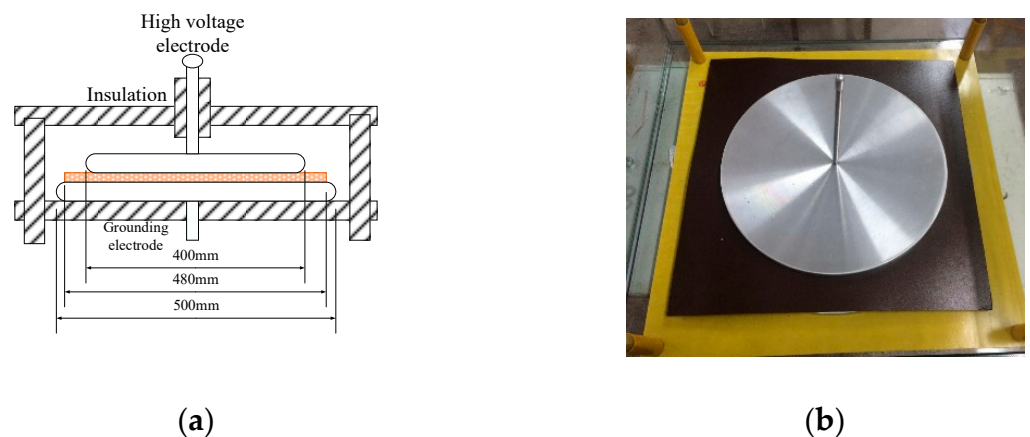


**Figure 1.** Schematic show and constructed setup for testing. (a) Schematic of test setup; (b) Picture of test setup.

### 2.2. Sample Preparation

The samples were prepared as in Figure 2. After cutting and drying, the samples are humidified to have different water content. The samples are weighed when the humidifying process is finished. With the weight difference, water content is calculated. It is obtained that the water contents for sample B and C are 2.4% and 3.8% separately. While A is the sample without water. More than three samples for each category (A, B, C) were prepared. However, only one test result for each is shown here since they are similar.

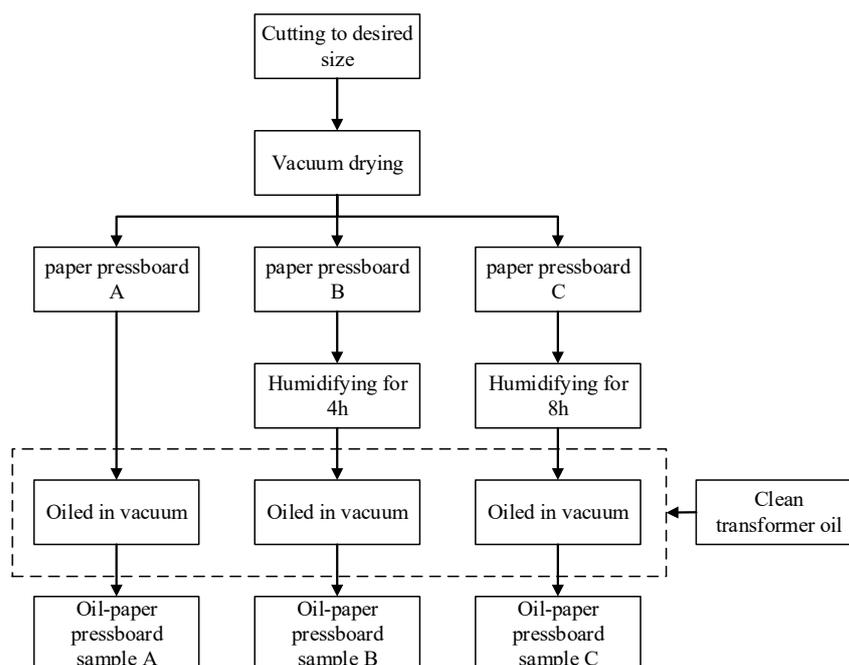


**Figure 2.** Sample preparation with different water content.

### 2.3. Data Extraction

Figure 3 shows the setup. The rated voltage of testing transformer is 110 kV and its apparent discharge is less than 5 pC. The protection resistor is 10 kΩ. The ratio of voltage divider is 1500:1. A high frequency current probe (HFCT) is used to measure the PD signal. The bandwidth of HFCT is 100 kHz–100 MHz with 1 pC sensitivity. The dielectric loss is characterized by  $\tan\delta$ , which is calculated as (1) by measuring the applied voltage and leakage current, where  $\varphi_i$  is the current phase for 50 Hz and  $\varphi_u$  is the voltage phase for 50 Hz. The calculation is performed based on FFT spectrum analysis. The Blackman–Harris window and interpolation technique were applied to eliminate the picket fence effect and leakage spectrum's effect on FFT, as in [24].

$$\tan \delta = \tan[\pi/2 - (\varphi_i - \varphi_u)] \quad (1)$$

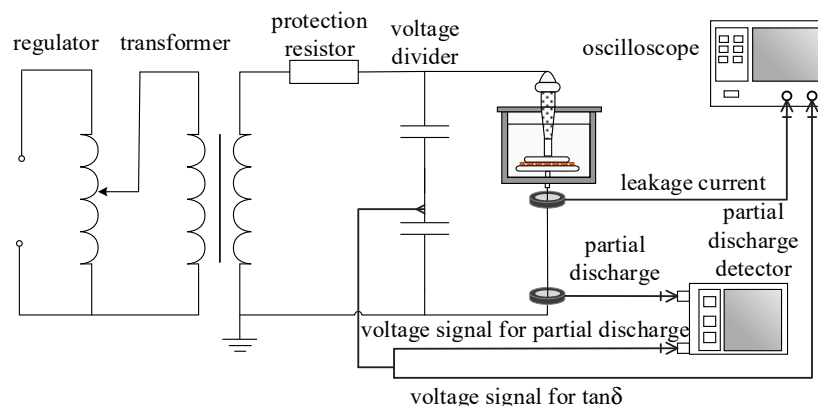


**Figure 3.** Setup of partial discharge and  $\tan\delta$  measurement.

The leakage current is measured with microammeter, whose measurement range is from 100  $\mu\text{A}$  to 700 mA and angle error is within  $\pm 0.01^\circ$ . The partial discharge detector's sampling frequency is 1 MHz. The test setup fulfills IEC60270. Shielding is considered in

the laboratory to guarantee a noise level lower than 5 pC. Dedicated error analysis can be nontrivial [25] and out of the scope of this paper.

Corresponding to Figure 4, the testing procedure is designed, as following:

1. apply 2 kV under which there is no PD. Record voltage and current signal for  $\tan\delta$  calculation;
2. increase voltage with 1 kV step and keep it stable for 1 min;
3. record PD and  $\tan\delta$  data for 5 min.  $\tan\delta$  data is registered each 30 s, thus 10 data are gathered in 5 min. PD is measured every 6s with recording length of 20 ms, leading to 50 data;
4. decrease the voltage to 2 kV and keep it for 1 min;
5. keep the voltage to be 2 kV for 2.5 min while gathering  $\tan\delta$  data. 5 data are recorded with 30 s time step; and,
6. repeat 2–5 until the voltage reaches  $0.8 \times U_b$  (flashover voltage). For sample group A, the stop voltage is 16 kV. For sample group B and C, the stop voltages are 14 kV and 12 kV.

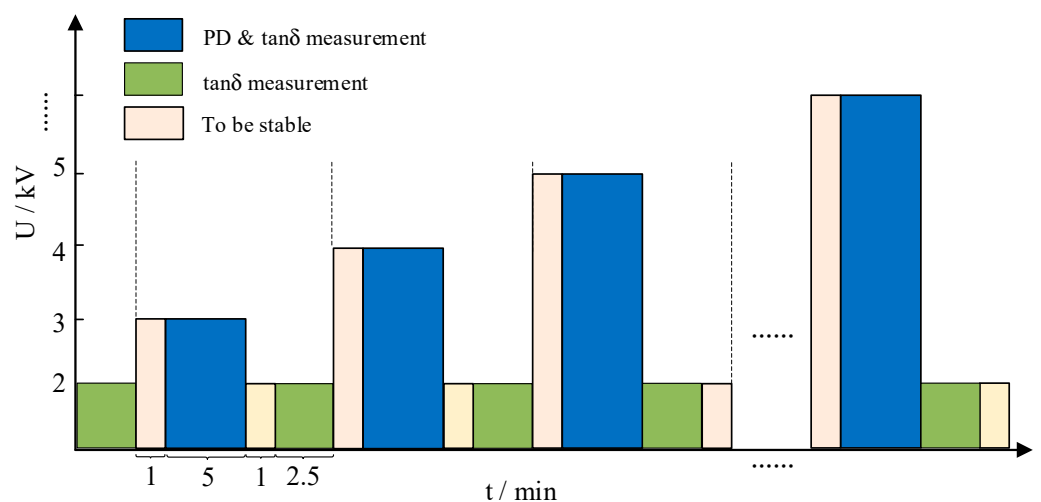


Figure 4. Setup of partial discharge and  $\tan\delta$  measurement.

### 3. Dielectric Loss and Partial Discharge Statistical Parameters

In order to study the correlation between PD and  $\tan\delta$ , firstly their own statistical parameters are analyzed, as below.

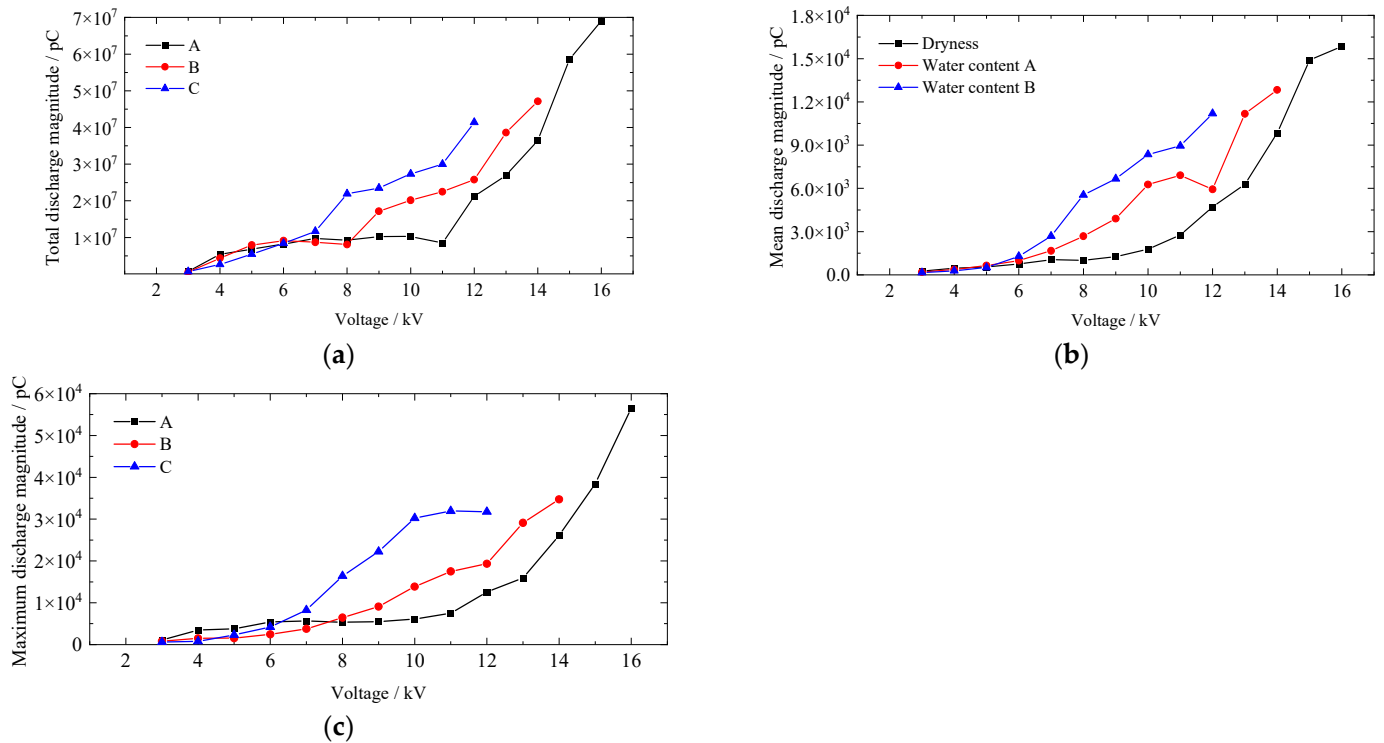
#### 3.1. PD Statistical Parameters

Table 1 lists the derived parameters, provided that  $H_n(q)$  is the phase-resolved data consisted of charge transfer  $q$ , and discharge rate  $n$ .

Table 1. Derived parameters for PD measurement.

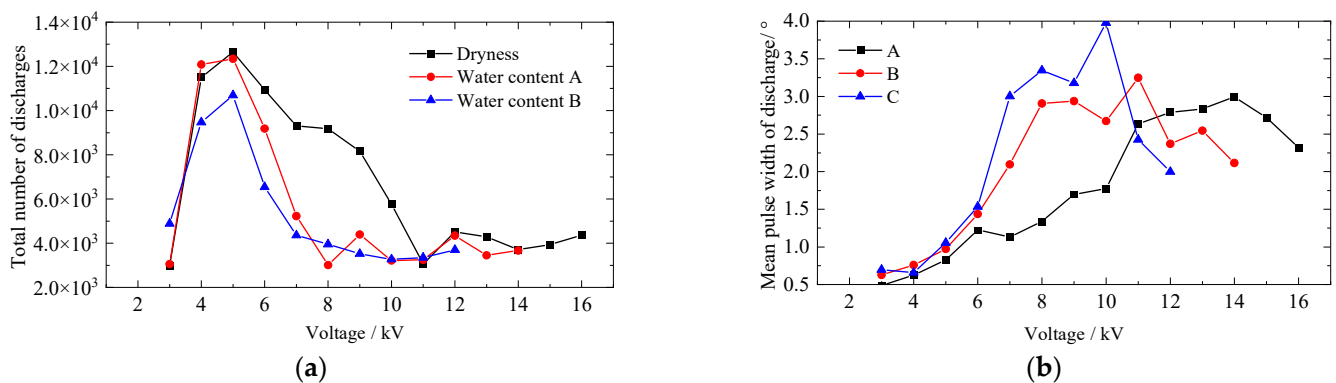
Parameter	Unit	Meaning
$q_t$	pC	total discharge magnitude
$n_t$	-	total number of discharges
$q_{avg}$	pC	mean discharge magnitude
$q_{max}$	pC	maximum discharge magnitude
$\sigma$	°	mean pulse width of discharge
$Sk$	-	skewness of $H_n(q)$
$Ku$	-	kurtosis of $H_n(q)$
$\alpha$	-	Weibull scale parameter of $H_n(q)$
$\beta$	-	Weibull shape parameter of $H_n(q)$

Figure 5a shows the total discharge magnitude  $q_t$ . Partial discharge increased with voltage and higher water content leads to more discharge. Mean discharge magnitude and maximum discharge magnitude with voltage are shown in Figure 5b,c with a similar trend.



**Figure 5.** (a) Relation between total discharge magnitude and voltage; (b) Relation between mean discharge magnitude and voltage; (c) Relation between maximum discharge magnitude and voltage.

Figure 6a shows the total number of discharges, which indicates that the voltage increase firstly enhanced the PD number and then hindered it. For the increase part, the water content did not have significant effect on the result. However, in the PD decrease part, water content lowered the PD occurring. Figure 6b is the mean width of discharge variation with voltage. It can be seen that, with the increase of voltage, the discharge duration firstly increased and then decreased. For the increase part, water content has positive effect on the pulse duration.



**Figure 6.** (a) Relation between total number of discharges and voltage; (b) Relation between mean pulse width of discharge and voltage.

Figure 7a,b show the skewness and kurtosis of  $H_n(q)$ . These two variables decreased with voltage, while water content also lowered the values. Figure 8 plots the Weibull parameters of  $H_n(q)$ . Figure 8a clearly shows that water content affected the scale parameter  $\alpha$  above 7 kV. Higher water content referred to bigger  $\alpha$ . Figure 8b shows the shape parameter  $\beta$ . For samples with water content,  $\beta$  shows a moderate decrease with the voltage. In contrast, this parameter increases a bit with voltage for samples without water.

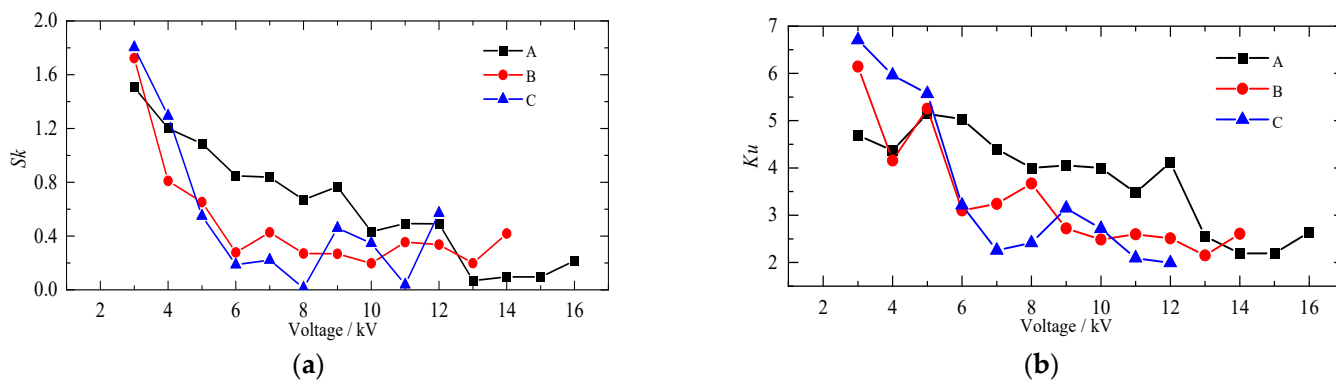


Figure 7. (a) Relation between skewness of  $H_n(q)$  and voltage; (b) Relation between kurtosis of  $H_n(q)$  and voltage.

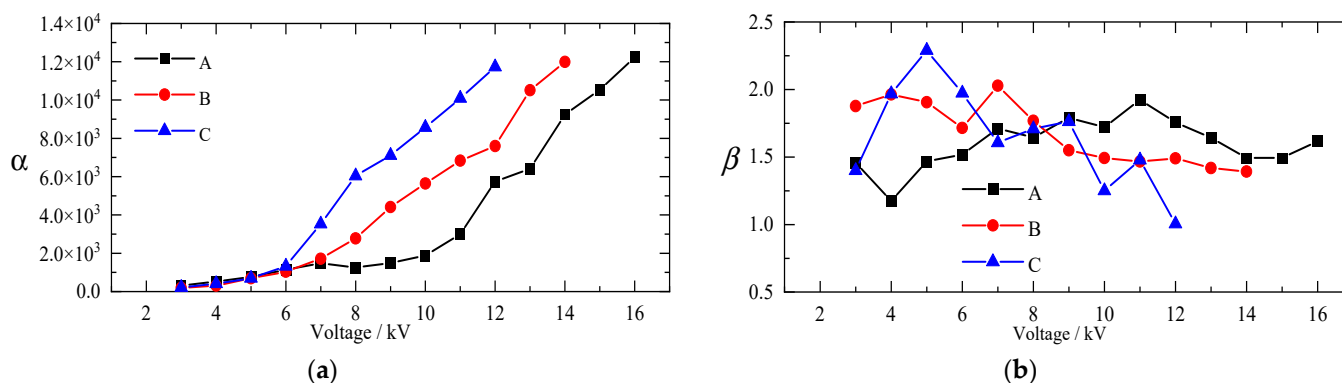


Figure 8. (a) Weibull scale parameter of  $H_n(q)$ ; (b) Weibull shape parameter of  $H_n(q)$ .

### 3.2. $\tan\delta$ Statistical Parameters

The average  $\tan\delta$  from step 3 and 5 in Section 2.3 was calculated and is shown in Figure 9. This value increased with voltage and water content. Additionally, there is clear difference for  $\tan\delta$  between Figure 9a,b, which indicates the dielectric loss variation before and after the voltage application.

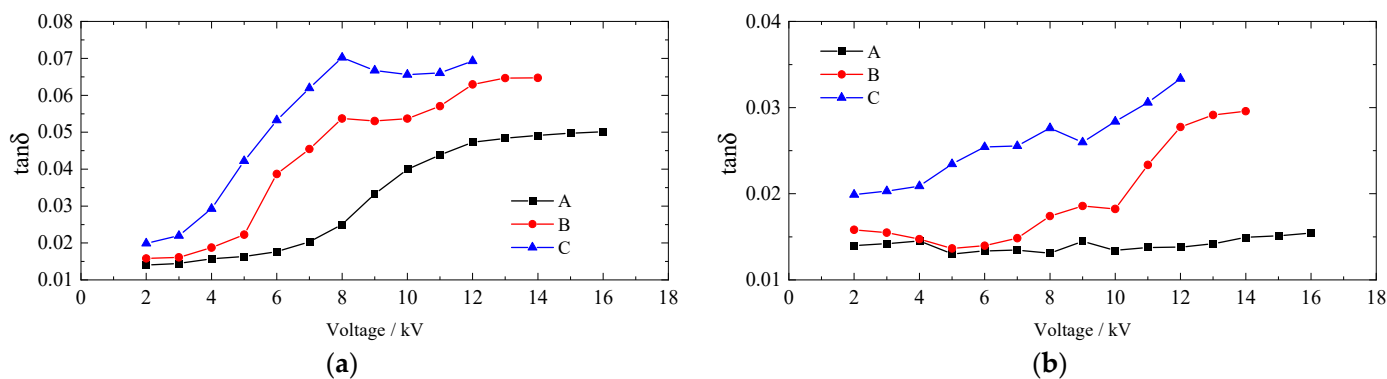


Figure 9. (a)  $\tan\delta$  after rise to different voltages; (b)  $\tan\delta$  at rested 2kV after rise to different voltages.

The difference between these two  $\tan\delta$  is obtained as Equation (2) and it is shown in Figure 10, where  $\tan\delta^U$  is the result in Figure 9a and  $\tan\delta_{2kV}^U$  is the result in Figure 9b. It can be seen that the voltage had positive effect on  $\tan\delta$  increase. While under the same voltage,  $\tan\delta$  increase has a positive dependency on water content.

$$\Delta \tan \delta = \tan \delta^U - \tan \delta_{2kV}^U \tag{2}$$

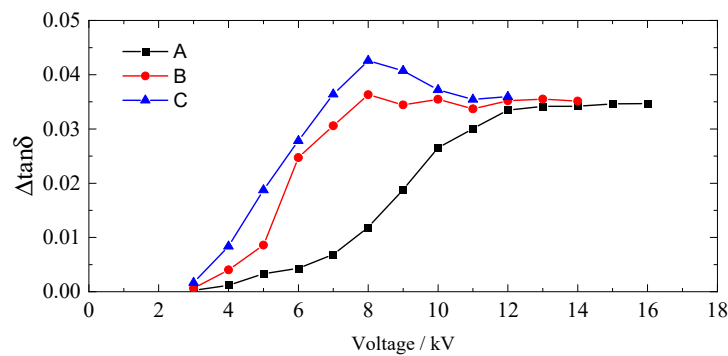


Figure 10. Dependency of  $\Delta \tan\delta$  with voltage.

To analyze the  $\tan\delta$  result, an equivalent circuit, as in Figure 11, is proposed. The grey block represents the defect area. The dielectric can be modelled by the double layer structure, as in the left figure of Figure 11, where layer I has defect and its equivalent parameters are  $R_1, C_1$  while layer II has no defect with equivalent parameters  $R', C'$ . Obviously, these two layers have different equivalent parameters. Layer II without defect has better insulation capability than layer I with defect. Thus,  $R' \gg R_1$ , and  $R'$  can be neglected, leading to the circuit in the right part of Figure 11. When voltage  $U_0$  is applied, current can be deduced as:

$$I = U_0 \frac{\omega^2 C_1^2 R_1 + j[\omega C' + \omega^3 C_1 C' (C_1 + C') R_1^2]}{1 + \omega^2 (C_1 + C')^2 R_1^2} \tag{3}$$

here  $\omega = 2\pi f$  and  $f$  is frequency.

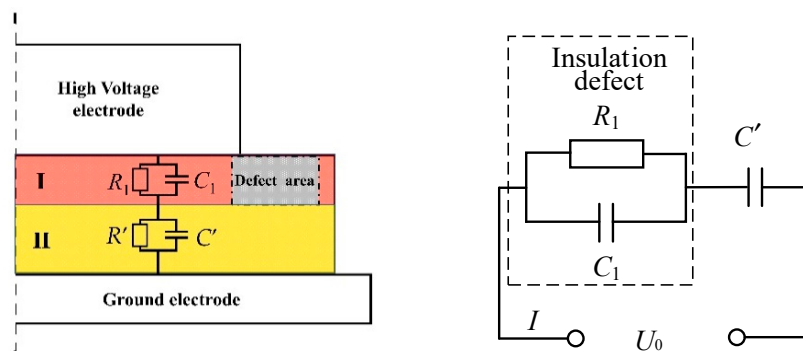


Figure 11. Equivalent circuit model of insulation with defect.

Based on Equation (3),  $\tan\delta$  can be expressed as:

$$\tan \delta = \frac{1/(\omega R_1 C_1)}{\frac{C_1}{C'} (1 + \frac{1}{\omega^2 C_1^2 R_1^2}) + 1} = \frac{\tan \delta_d}{H(1 + \tan \delta_d^2) + 1} \tag{4}$$

where  $H = C_1/C'$  and it is defined as defect factor. When the defect is enlarged,  $C_1$  decreases (layer I gets thicker) and  $C'$  increases, which makes  $H$  smaller.  $\tan\delta_d$  is the dielectric loss

for defect part. When  $\tan\delta_d$  is constant,  $\tan\delta$  is reversely related with  $H$ . Figure 12 shows the dependency of  $\tan\delta$  with  $\tan\delta_d$  and  $H$ , where  $H_1 < H_2 < H_3$ .

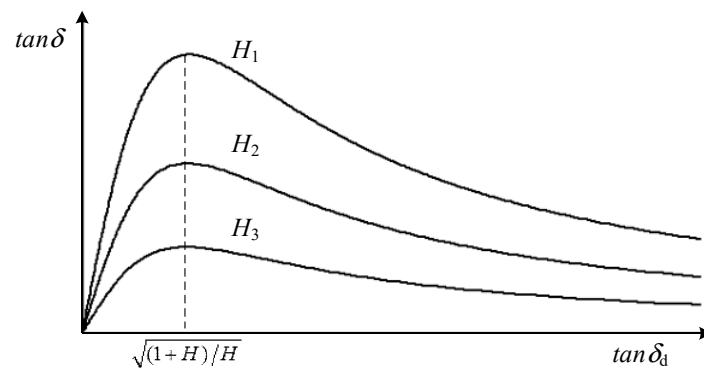


Figure 12.  $\tan\delta$  of insulation characteristic upon defect factor  $H$  and  $\tan\delta_d$ .

Figure 13 is the  $\tan\delta$  characteristic of sample A. Figure 13a is the measured result and Figure 13b is the ideal  $\tan\delta$  curve for sample A based on Figure 12. When the voltage was lower than 6 kV, PD did not show up severely, both  $\tan\delta_d$  and  $H$  did not vary much, making  $\tan\delta$  increase gently. For the voltage from 7 kV–12 kV, due to PD's effect, the defect's dielectric loss  $\tan\delta_d$  increased. Yet, the defect area did not increase much, which means that  $H$  did not change. This can be confirmed by the rather stable curve for sample A in Figure 9b between 7 kV and 12 kV (after voltage application, dielectric loss did not change). Thus,  $\tan\delta$  increased sharply in this range. For voltage above 12 kV,  $H$  decreased, which can be seen in Figure 9b for the rise above 12 kV. Additionally,  $\tan\delta_d$  increased due to continuous PDs. The combined effect changed the curve from A to B, then to C, as in Figure 13b.

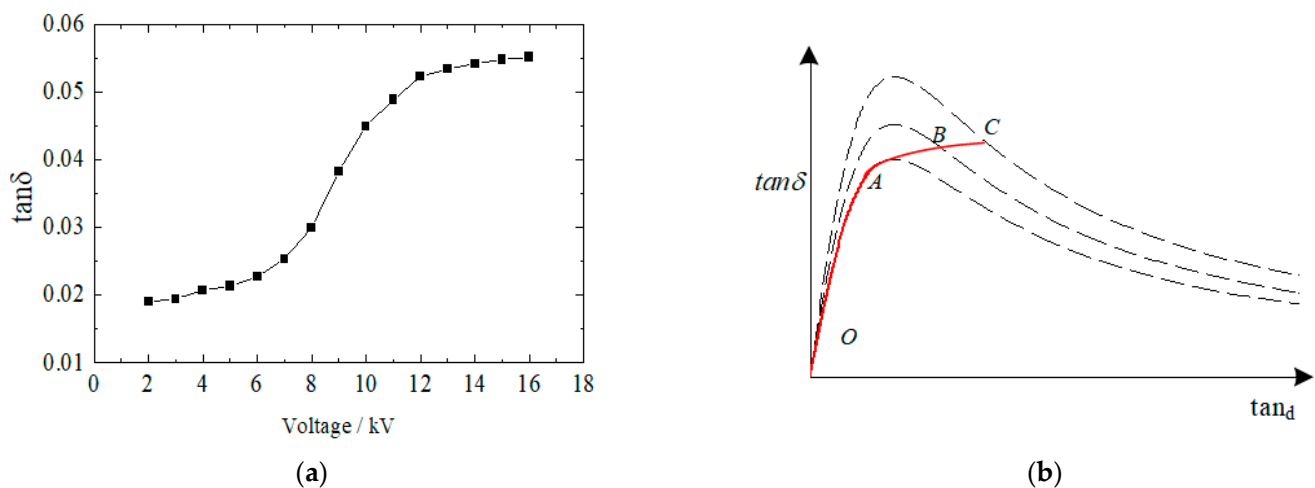


Figure 13. (a)  $\tan\delta$  characteristic of sample A; (b) Schematic ideal  $\tan\delta$  characteristic for sample A.

For sample B and C, the  $\tan\delta$  characteristic is analyzed in Figure 14 by taking sample B as an example. There is a tuning point of about 8 kV. This can be explained as  $\tan\delta_d$ 's increase surpassed the peak, as in Figure 12, due to water effect. If  $H$  keeps constant, then the curve decreased (from 8 kV to 10 kV in Figure 14a and point A to B in Figure 14b). With the continuous voltage rise, PD enlarged the defect and lowered the defect factor  $H$ . Together with the increase of  $\tan\delta_d$  due to PD's effect, the curve shown in Figure 14a increased above 10 kV and the curve in Figure 14b changed from B to D.

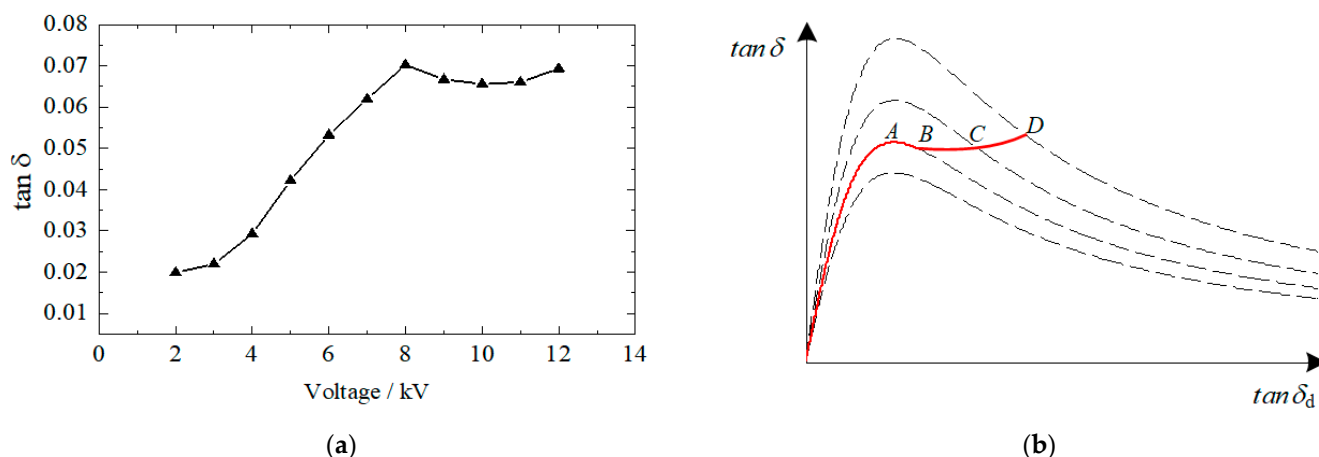


Figure 14. (a)  $\tan\delta$  characteristic of sample B; (b) schematic ideal  $\tan\delta$  characteristic for sample B.

#### 4. Correlation between PD and Tan $\delta$

The correlation between PD and  $\tan\delta$  is studied by Pearson’s coefficient. For vector  $x = (x_1, x_2, \dots x_n)$  and  $y = (y_1, y_2, \dots y_n)$ , Pearson’s coefficient is calculated, as below:

$$r = \frac{\sum_{i=1}^n \left(x_i - \frac{1}{n} \sum_{i=1}^n x_i\right) \left(y_i - \frac{1}{n} \sum_{i=1}^n y_i\right)}{\sqrt{\sum_{i=1}^n \left(x_i - \frac{1}{n} \sum_{i=1}^n x_i\right)^2 \sum_{i=1}^n \left(y_i - \frac{1}{n} \sum_{i=1}^n y_i\right)^2}} \tag{5}$$

when  $r$  is 1, the two vectors are completely positively correlated. When  $r$  is  $-1$ , the two vectors are completely negatively correlated.

##### 4.1. Correlation between PD and $\tan\delta$ Statistical Parameters

Table 2 lists the calculated correlation coefficients. All of the shown absolute values are above 0.7, which indicates strong correlation. The detailed data are listed in Figure 15. As in the Figure, although disturbance is observed, correlation is clear between dielectric loss and PD.

Table 2. Correlation coefficient with  $\tan\delta$ .

	$q_t$	$n_t$	$q_{avg}$	$q_{max}$	$\sigma$	$Sk$	$Ku$	$\alpha$
A	0.728	-0.734	0.767	0.712	0.962	-0.734	-0.818	0.718
B	0.804	-0.709	0.819	0.809	0.871	-0.762	-0.812	0.744
C	0.837	-0.708	0.808	0.796	0.847	-0.770	-0.837	0.766

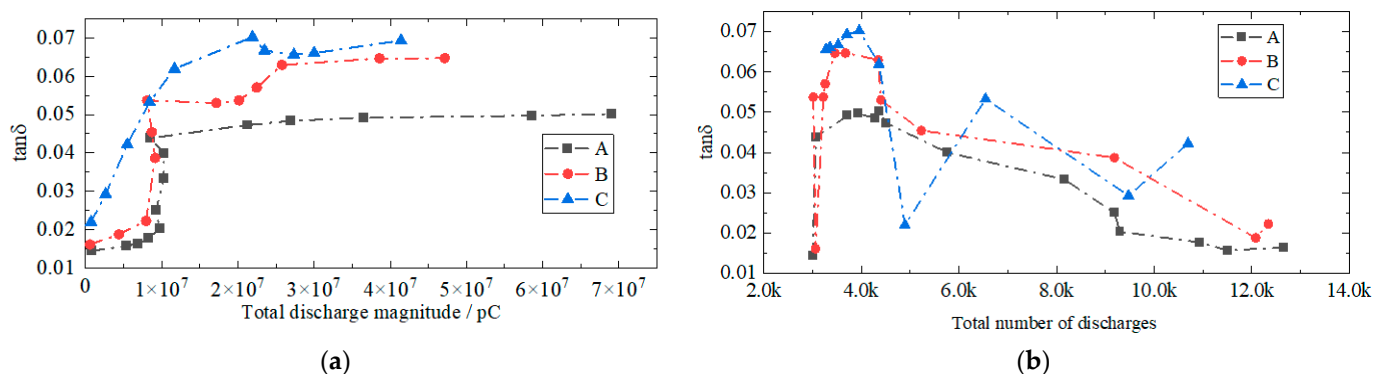
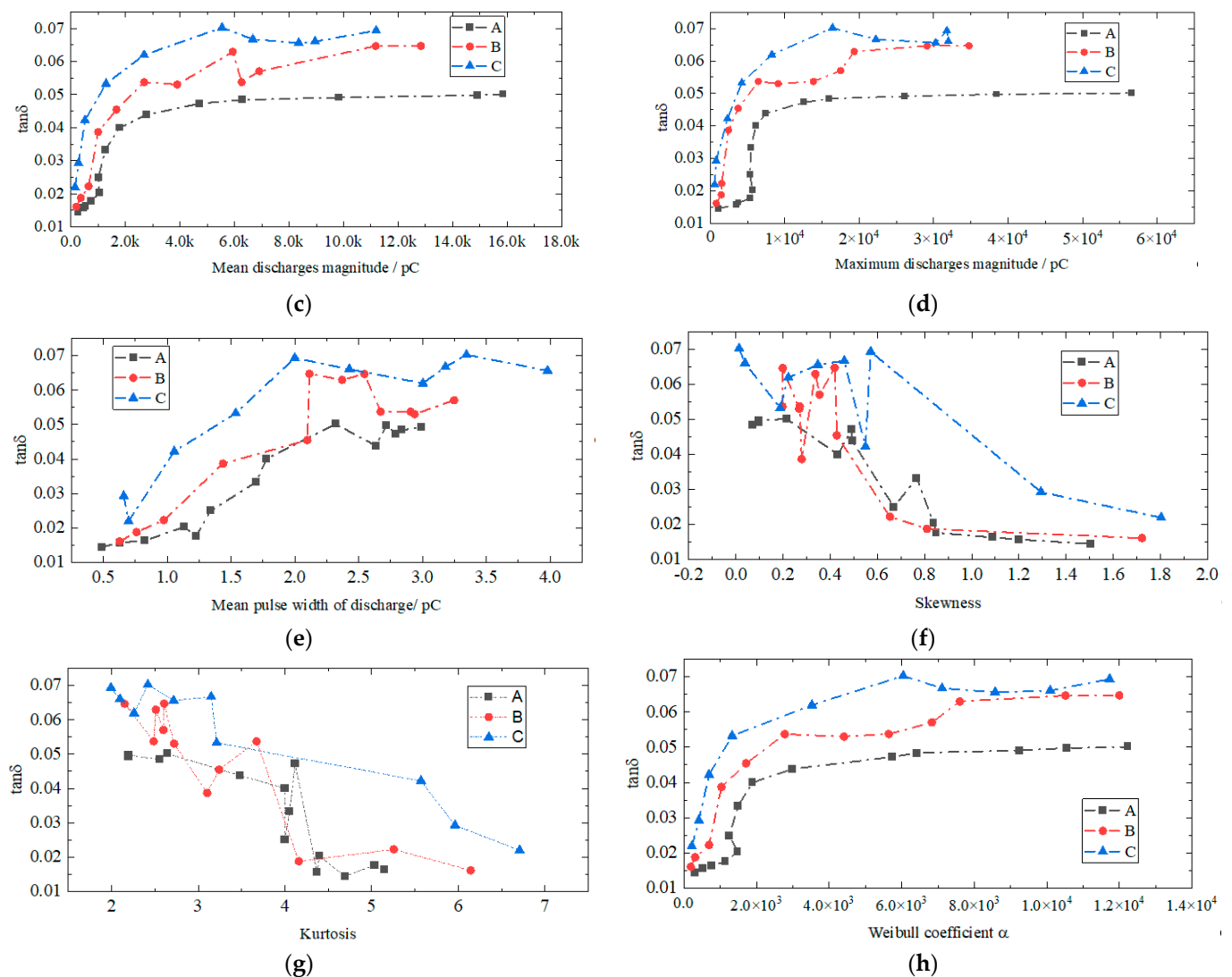


Figure 15. Cont.



**Figure 15.** (a) Total discharge magnitude with  $\tan\delta$ ; (b) Total number of discharges with  $\tan\delta$ ; (c) Mean discharges magnitude with  $\tan\delta$ ; (d) Maximum discharges magnitude with  $\tan\delta$ ; (e) Mean pulse width of discharge with  $\tan\delta$ ; (f) Skewness of  $H_n(q)$  with  $\tan\delta$ ; (g) Kurtosis of  $H_n(q)$  with  $\tan\delta$ ; and, (h) Weibull coefficient of  $H_n(q)$  with  $\tan\delta$ .

#### 4.2. Correlation between PD and $\Delta\tan\delta$

Because no PD was observed when the voltage was lowered to 2 kV, as in Figure 4,  $\Delta\tan\delta$  can be regarded as the effect the PD during voltage rise.

$\tan\delta$  is derived from 50 Hz voltage and current. When there is PD containing 50 Hz component, it will affect the  $\tan\delta$  result. Thus, the 50 Hz component was taken from the PD signal and normalized. The result is compared with  $\tan\delta$  and shown in Figure 16. It can be seen that there is strong correlation between these two variables.

This correlation can be further observed in Figure 17, where a linear relation is shown. To further analyze this phenomenon, PD is simulated based on measured data. Figure 18 shows the typical recorded waveform of PD with reference voltage. The PDs occurred at 0–90° and 180–270°, and they were basically symmetric in the positive and negative cycles. With increase of applied voltage, PD grew, and it covered wider phase range, as in Figure 18b as compared with Figure 18a. For case of ease, the following assumptions are taken for simulated PDs:

1. PDs occur symmetrically with respect to positive and negative cycles;
2. square wave is used to simulate PDs;
3. all PDs have the same amplitude, duration and repetition rate; and,

4. in the positive cycle, the PDs are centered at  $45^\circ$ , while, in the negative cycle, the PDs are centered at  $225^\circ$ .

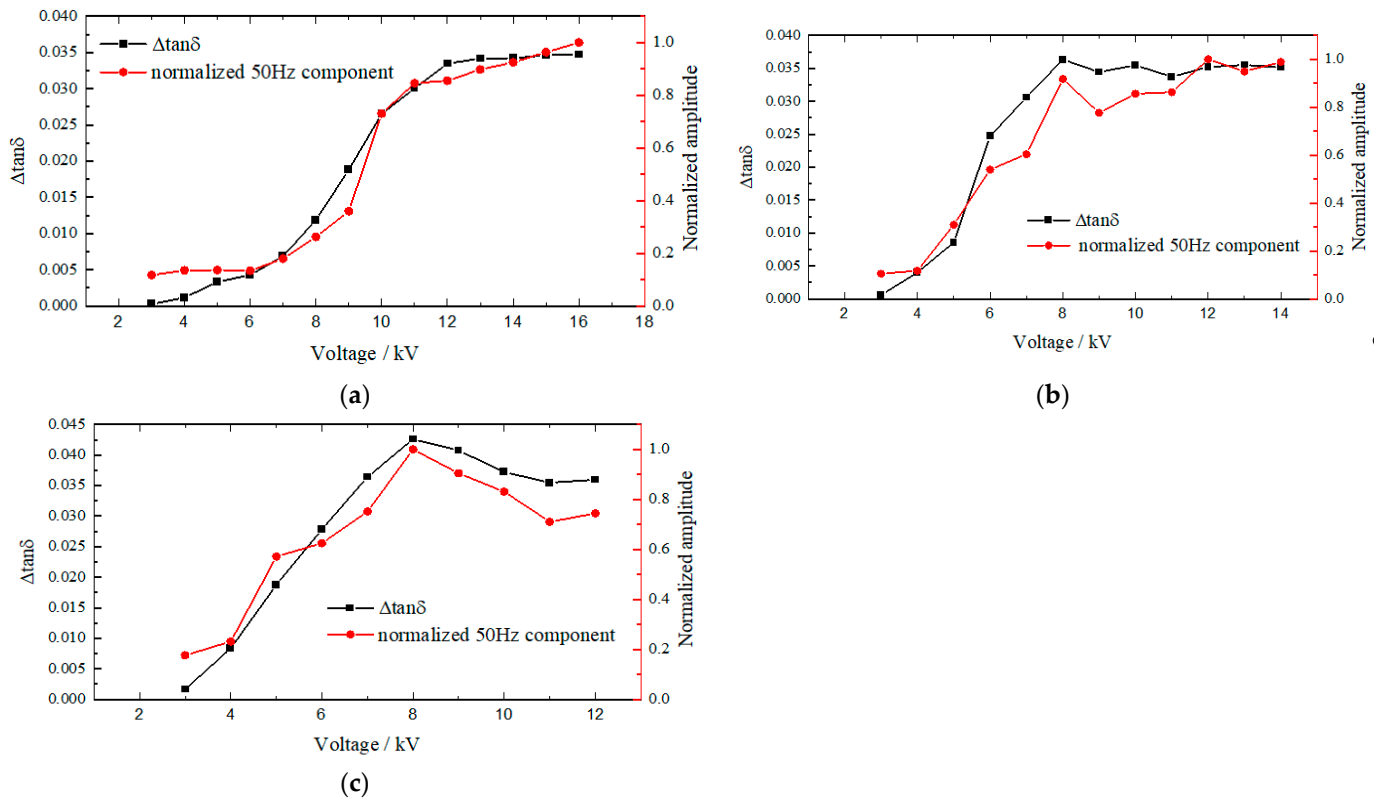


Figure 16. Comparison between  $\tan \delta$  and normalized 50 Hz component from PDs. (a) is for sample A, (b) is for sample B, and (c) is for sample C.

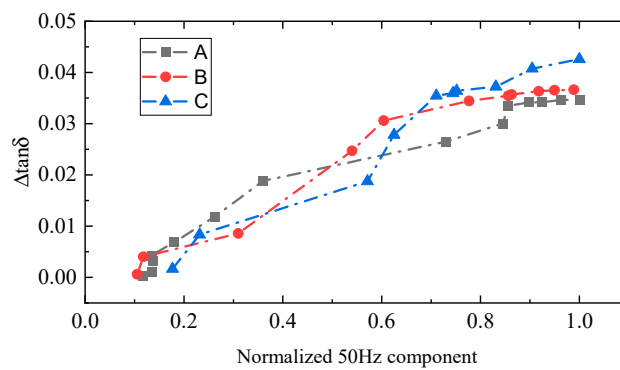


Figure 17. Relation between  $\Delta \tan \delta$  and normalized 50 Hz component from PDs.

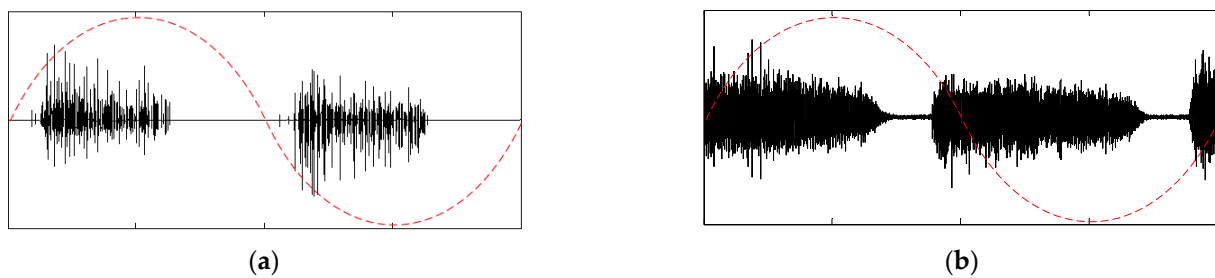


Figure 18. (a) Measured PD signal with reference voltage; (b) Measured PD signal with higher reference voltage.

Figure 19 shows the simulated PDs. Three simulation tests are performed.

1. PD amplitude  $A$  is set to 1. PD duration is set to be  $10\ \mu\text{s}$ . The time interval between each PD is  $20\ \mu\text{s}$ . The number of PDs is set to be 20, 40, and 60. Their effect to the frequency component is analyzed, as in Figure 20. It shows that, with the increase of PD number, the 50 Hz component is also increased.
2. PD duration is set to be  $10\ \mu\text{s}$ . The time interval between each PD is  $20\ \mu\text{s}$ . The number of PDs is set to be 20. While PD amplitude  $A$  is set to be 1–3. Their effect on the frequency component is analyzed, as in Figure 21. Additionally, the amplitude rise will increase the 50 Hz component.
3. PD amplitude  $A$  is set to 2. The time interval between each PD is  $20\ \mu\text{s}$ . The number of PDs is set to be 40. While PD duration varies as  $10\ \mu\text{s}$ ,  $20\ \mu\text{s}$ , and  $30\ \mu\text{s}$ . Their effect on the frequency component is analyzed, as in Figure 22. Again, the duration enlargement will increase the 50 Hz component.

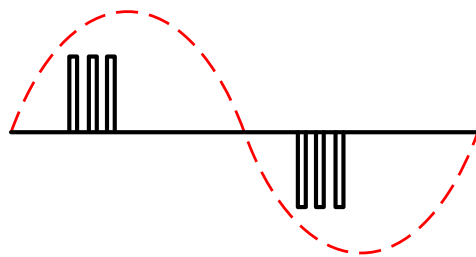


Figure 19. Simulated PDs with reference voltage.

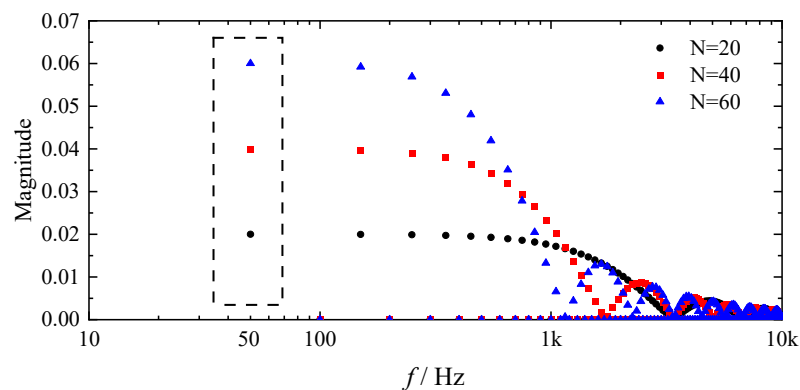


Figure 20. Total number of discharge effect on PD's amplitude-frequency result.

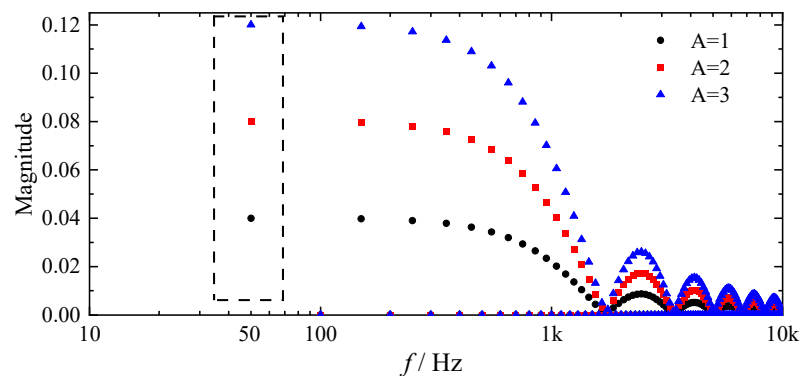
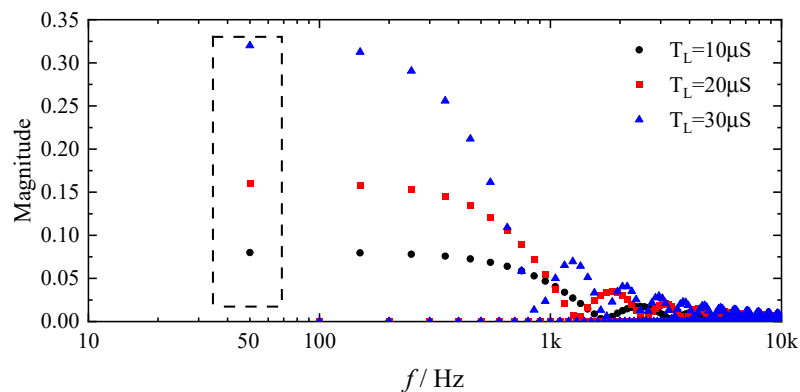


Figure 21. Discharge magnitude effect on PD's amplitude-frequency result.



**Figure 22.** Pulse duration of discharge effect on PD's amplitude-frequency result.

## 5. Conclusions

For oil-pressboard insulation, the discharge magnitude rises with voltage and water content. Dielectric loss  $\tan\delta$  increased with voltage. However, there is saturation. For oil-pressboard with water,  $\tan\delta$  can even decrease with voltage. An equivalent circuit model is proposed to explain this characteristic, which shows that  $\tan\delta$  is dependent on defect area and the dielectric loss of defect part.

Dielectric loss  $\tan\delta$  is correlated with PD, specifically with total discharge magnitude, total number of discharges, average discharge magnitude, maximum discharge magnitude, average pulse duration of discharge, Weibull scale parameter, skewness, and kurtosis of phase-resolved data consisting of charge transfer and discharge rate. The dielectric loss difference that is obtained from  $\tan\delta$  at raised voltages and rested 2 kV is almost linearly correlated with and contributed by 50 Hz component of PDs.

The strong correlations between dielectric loss and PD, especially between the dielectric loss difference and 50 Hz component of PDs, improves the degradation's understanding and provides a diagnostic tool for oil-pressboard that helps to eliminate the information asymmetry from single parameter. With the derived data and model, one can observe the correlation between  $\tan\delta$  and PD, with which further study of the degradation process of the oil-pressboard insulation material can be performed, and a multi-source information fusion insulation evaluation technique can be developed to improve the power equipment assessment level.

**Author Contributions:** Conceptualization, M.L. and J.X.; methodology, J.X.; software, J.X.; validation, Y.L., M.L. and J.X.; formal analysis, J.X.; investigation, J.X.; resources, M.L.; data curation, M.L.; writing—original draft preparation, M.L.; writing—review and editing, Y.L.; visualization, Y.L.; supervision, J.X.; project administration, J.X.; funding acquisition, Y.L. All authors have read and agreed to the published version of the manuscript.

**Funding:** This research was funded by the Fundamental Research Funds for the Central Universities, grant number 2018MS081.

**Institutional Review Board Statement:** Not applicable.

**Informed Consent Statement:** Not applicable.

**Data Availability Statement:** The data presented in this study are available on request from the corresponding author.

**Conflicts of Interest:** The authors declare no conflict of interest.

## References

- Zhou, X.; Werle, P.; Gockenbach, E.; Shi, H.; Kuhnke, M. Study of Oil/Pressboard Creeping Discharges under Divergent AC Voltage—Part 1: Fundamental Phenomena and Influencing Factors. *IEEE Trans. Dielectr. Electr. Insul.* **2021**, *28*, 355–363. [CrossRef]
- Zhou, L.; Liao, W.; Wang, D.; Wang, D.; Zhang, G.; Cui, Y.; Cai, J. A High-Precision Diagnosis Method for Damp Status of OIP Bushing. *IEEE Trans. Instrum. Meas.* **2021**, *70*, 1–10. [CrossRef]

3. Okabe, S.; Koto, M.; Muraoka, T.; Suganuma, K.; Takahashi, K. Techniques for diagnosing deterioration of oil-impregnated paper-film power capacitors. *IEEE Trans. Power Deliv.* **1997**, *12*, 1751–1759. [[CrossRef](#)]
4. Garzem, M.; Grunwald, M.; Schnorrenberg, R.; Schumacher, R.; Humpert, C. Breakdown and Partial Discharge Characteristics of Transformer Board and Insulating Paper Materials in Liquid Nitrogen. *IEEE Trans. Appl. Supercond.* **2018**, *28*, 1–5. [[CrossRef](#)]
5. Rajnak, M.; Timko, M.; Kopcansky, P.; Paulovicova, K.; Kuchta, J.; Franko, M.; Kurimsky, J.; Dolnik, B.; Cimbala, R. Transformer oil-based magnetic nanofluid with high dielectric losses tested for cooling of a model transformer. *IEEE Trans. Dielectr. Electr. Insul.* **2019**, *26*, 1343–1349. [[CrossRef](#)]
6. Mohsin, M.M.; Narayanachar, M.N.; Nema, R.S. A study of partial discharge characteristics in oil impregnated pressboard insulation. In Proceedings of the IEEE International Symposium on Electrical Insulation, Montreal, QC, Canada, 16–19 June 1996; pp. 79–82.
7. Takahashi, E.; Tsutsumi, Y.; Okuyama, K.; Ogata, F. Partial discharge characteristics of oil-immersed insulation systems under DC, combined AC-DC and DC reversed polarity voltage. *IEEE Trans. Power Appar. Syst.* **1976**, *95*, 411–420. [[CrossRef](#)]
8. Burkas, P.D.; Stathopoulos, I.A. Partial discharges in the pressboard-oil insulation under switching impulse voltages. In Proceedings of the Fifth International Symposium on High Voltage Engineering, Braunschweig, Germany, 24–28 August 1987; pp. 1–4.
9. Wasilenko, E.; Wesolowski, H. Influence of switching impulses on development of partial discharges in oilimpregnated paper insulation. In Proceedings of the Second International Conference on Properties and Applications of Dielectric Materials, Beijing, China, 12–16 September 1988; pp. 90–93.
10. Raja, K.; Nema, R.S. Comparative statistical aging studies on an oil-pressboard insulation model. In Proceedings of the 5th International Conference on Properties and Applications of Dielectric Materials, Seoul, Korea, 25–30 May 1997; pp. 259–262.
11. Sahoo, N.C.; Salama, M.M.A.; Bartnikas, R. Trends in partial discharge pattern classification: A survey. *IEEE Trans. Dielectr. Electr. Insul.* **2005**, *12*, 248–264. [[CrossRef](#)]
12. Ruan, J.; Xie, Y.; Jin, S.; Shi, Y.; Tian, Y.; Deng, Y. Inversion of Oil-Immersed Paper Resistivity in Transformer Based on Dielectric Loss Factor. *IEEE Access* **2019**, *7*, 44050–44058. [[CrossRef](#)]
13. Yang, X.; Nielsen, S.; Ledwich, G. Frequency domain spectroscopy measurements of oil-paper insulation for energized transformers. *IEEE Trans. Dielectr. Electr. Insul.* **2017**, *24*, 1657–1664. [[CrossRef](#)]
14. Li, J.; Zhang, Z.; Grzybowski, S.; Zahn, M. A new mathematical model of moisture equilibrium in mineral and vegetable oil-paper insulation. *IEEE Trans. Dielectr. Electr. Insul.* **2012**, *19*, 1615–1622. [[CrossRef](#)]
15. Badicu, L.V.; Gorgan, B.; Dumitran, L.M.; Notingher, P.V. Assessment of transformer mineral oil condition based on dc and ac conductivity. *IEEE Trans. Dielectr. Electr. Insul.* **2012**, *19*, 1544–1551. [[CrossRef](#)]
16. Liu, J.; Fan, X.; Zhang, C.; Lai, C.S.; Zhang, Y.; Zheng, H.; Lai, L.L.; Zhang, E. Moisture diagnosis of transformer oil-immersed insulation with intelligent technique and frequency-domain spectroscopy. *IEEE Trans. Ind. Informatics* **2021**, *17*, 1. [[CrossRef](#)]
17. Przybyłek, P.; Nadolny, Z.; Moscicka-Grzesiak, H. Bubble effect as a consequence of dielectric losses in cellulose insulation. *IEEE Trans. Dielectr. Electr. Insul.* **2010**, *17*, 913–919. [[CrossRef](#)]
18. Cui, Y.; Ma, H.; Saha, T.; Ekanayake, C. Understanding Moisture Dynamics and Its Effect on the Dielectric Response of Transformer Insulation. *IEEE Trans. Power Deliv.* **2015**, *30*, 2195–2204. [[CrossRef](#)]
19. Liao, R.; Du, Y.; Yang, L.; Gao, J. Quantitative diagnosis of moisture content in oil-paper condenser bushing insulation based on frequency domain spectroscopy and polarisation and depolarisation current. *IET Gener. Transm. Distrib.* **2017**, *11*, 1420–1426. [[CrossRef](#)]
20. Rowland, S.; Wang, M. Fault Development in Wet, Low Voltage, Oil-Impregnated Paper Insulated Cables. *IEEE Trans. Dielectr. Electr. Insul.* **2008**, *15*, 484–491. [[CrossRef](#)]
21. Ramya, M.; Udayakumar, K. Characterization of partial discharge phenomenon on paper insulation under aggravated aging conditions. In Proceedings of the 2002 IEEE 14th International Conference on Dielectric Liquids, ICDL 2002, Graz, Austria, 7–12 July 2002; pp. 433–436.
22. Zupan, T.; Mikulecky, A.; Ziger, I. Ageing, Temperature and Water Content Influence on Oil-Paper Insulation: Model Preparation. In Proceedings of the 2018 IEEE 2nd International Conference on Dielectrics (ICD), Budapest, Hungary, 1–5 July 2018; pp. 1–4.
23. Jiang, J.P.; Du, B.X.; Cavallini, A. Effect of moisture migration on surface discharge on oil-pressboard of power transformers under cooling. *IEEE Trans. Dielectr. Electr. Insul.* **2020**, *27*, 1743–1751. [[CrossRef](#)]
24. Xu, Z.; Lu, F.; Li, H. Simulation analysis of dielectric loss angle measured by the Blackman-Harris window interpolation algorithm. *High Voltage Eng. (Chin.)* **2007**, *3*, 104–108.
25. Tomczyk, K. Procedure Proposal for Establishing the Class of Dynamic Accuracy for Measurement Sensors Using Simulation Signals with One Constraint. *Measurement* **2021**, *178*, 109367. [[CrossRef](#)]